ngVLA Antenna Memo #12
Verification Testing for the ngVLA 18 m Prototype Antenna

Jeff Mangum (NRAO)

January 11, 2022

Abstract

This document provides detailed information and corresponding analysis of measurement system options and associated procedures which will enable customer acceptance testing of the ngVLA 18 m prototype antenna. Detailed design and analysis of testing procedures for surface, pointing, and path length performance are provided, as these three performance requirements drive software and hardware development for the ngVLA 18 m antenna customer acceptance testing. Recommendations for how to perform surface, pointing, and path length performance measurements are provided.

1 Introduction

The ngVLA 18 m antenna site acceptance testing task list is provided in Table 11. This table is reproduced from Dunbar (2020), Section 16, Table 10, where we have extracted requirements that relate to antenna performance that will need to be verified during site acceptance testing. Many of the antenna performance requirements listed are rather straightforward to test (i.e. focus stability). Three exceptions are the performance requirements for surface accuracy, pointing, and path length stability. The verification of these three performance requirements are much more involved, requiring the development of measurement systems and techniques with sensitivity to surface deformation, pointing error, and path length error. In this memo we describe measurement systems, and their projected performance, which we believe will meet these requirements.

2 Environmental Conditions

The environmental conditions associated with precision, normal, and survival operating conditions are summarized in Table 1. A standard weather station with the capability to measure atmospheric pressure, ambient temperature, dew point temperature, and wind speed and direction will be sufficient to provide these environmental condition measurements. Note that all antenna performance requirements will need to be evaluated within their respective environmental conditions, limited by the availability of these environmental conditions during the antenna site acceptance testing period.

Table 1: ngVLA 18 m Environmental Condition Requirements

Op Env	Req #[a]	Value	Trace[a]	Eval Prec
Environmental Requirements				
Precision	ANT1412, ANT1413, ANT1414, ANT1415	$W_s \leq 5$ m/s average over 10 minutes with 7 m/s peak gusts; $-15 \leq T_{amb} \leq +25$ C; $\Delta T_{amb} \leq 1.8$ C/hr; no precip	ENV0312, ENV0313, ENV0314, ENV0315	Wx
Normal	ANT1422, ANT1423, ANT1424, ANT1425	$W_s \leq 7$ m/s average over 10 minutes with 10 m/s peak gusts; $-15 \leq T_{amb} \leq +25$ C; $\Delta T_{amb} \leq 3.6$ C/hr; no precip	ENV0322, ENV0323, ENV0324, ENV0325	Wx
Survival	ANT1441, ANT1442, ANT1443, ANT1444, ANT1445, ANT1446	$W_s \leq 50$ m/s; $-30 \leq T_{amb} \leq +52.5$ C; Ice ≤ 2.5 cm; Rain ≤ 16 cm/hr over 10 minutes; Snow ≤ 25 cm; Hail ≤ 2.0 cm	ENV0322, ENV0323, ENV0324, ENV0325	Wx/ manual

[a] See Dunbar (2020); Selina et al. (2018); Hales (2019).

3 Elevation and Azimuth Range Sampling

It is unnecessary, and for many tests impractical, to measure all antenna performance requirements at all azimuth and elevation angles. An estimate of the azimuth and elevation angle sampling sufficient to characterize the antenna performance requirements is as follows:

- Elevation: 12 degrees, every 15 degrees from 15 to 75 degrees, 88 degrees
- Azimuth: Every 60 degrees over the full ± 180 degree range

The sampling chosen in Az/El are based on typical performance dependence on each coordinate, with elevation often showing more performance dependence on several criteria to be evaluated. This implies that 7 elevation $\times$ 6 azimuth angles = 42 Az/El positions will need to be measured for most performance parameters. Note, though, that azimuth-dependent deformations which adversely affect pointing and surface performance are rare, so one can likely use a courser sampling of azimuth angles in practice.

4 Mechanical Requirements

The antenna mechanical requirements to be evaluated during prototype antenna site acceptance testing are summarized in Table 2. The antenna mechanical requirements listed here will actually be measured as a result of the pointing measurements (Section 7) through several pointing model terms.

Table 2: ngVLA 18 m Mechanical Requirements

Op Env	Req #[a]	Value	Trace[a]	Eval Prec
Axis Offsets				
All	ANT0205, ANT0206, ANT0207	Minimize all offsets: El-Boresight, Az-El, and Az-Boresight	CAL0313	Pointing

[a] See Dunbar (2020); Selina et al. (2018); Hales (2019).

5 Focus and Positioning Requirements

The antenna focus and positioning requirements to be evaluated during prototype antenna site acceptance testing are summarized in Table 3. Some of the antenna focus and positioning requirements listed here will actually be measured as a result of the pointing measurements (Section 7) as a by-product of the pointing measurement process. Specifically, the tests needed to verify each performance metric in Table 3 are as follows:

- Focus Stability
  - Manual measurement
  - Radiometric absolute and referenced pointing measurement
- Positioning Performance
  - Position sampling while performing radiometric absolute pointing measurements
  - Position sampling while tracking radiometric source

The antenna electronics installation at the secondary focus must employ the antenna vendor-provided feed indexer mechanism, and permit at least limited motion of the indexer in both axes to enable measurements of indexer repeatability, and to correctly include the indexer positioning error that would be typical from switching bands as part of referenced pointing. Enabling full translation of the indexer mechanism in both axes would be desirable.

Table 3: ngVLA 18 m Focus and Positioning Requirements

Op Env	Req #[a]	Value	Trace[a]	Eval Prec
Focus Stability and Performance				
All	ANT0702, ANT0703, ANT0704	$\Delta(X_f, Y_f, Z_f) = (2.2, 0.5, 0.5)$ mm; $\Delta\theta_f \leq 0.5$ deg; Transverse full range ≤ 10 sec	SYS1001, CAL0205, CAL0206	Manual/ Pointing
Positioning Performance				
All	ANT0901, ANT0902, ANT0903, ANT0904, ANT0905, ANT0906, ANT0907	Slew Az/El $\geq$ 90/45 deg/min; Accel Az/El $\geq$ 4.5/2.25 deg/sec^2; Slew 3 deg on sky and settle to within Referenced Pointing Requirement within 7 sec for El $<$ 70 deg; Tracking Az/El $\leq$ 7.5/3.5 deg/min	SYS1103, SYS3005, CAL0207, SYS1104	Pointing

[a] See Dunbar (2020); Selina et al. (2018); Hales (2019).

6 Surface Accuracy Requirement

In the following we describe the measurement systems and techniques which we believe will allow for the proper characterization of the ngVLA 18 m antenna surface performance. Table 4 lists these antenna performance requirements and the requirements for the associated measurement systems that NRAO will need to develop. The tests needed to verify the surface accuracy requirement are as follows:

- Antenna surface measurements at all required Az/El positions
- Adequate environmental condition sampling, especially at extremes of ambient temperature and wind speed conditions

Table 4: ngVLA 18 m Antenna Surface Requirements

Op Env	Req #[a]	Value	Trace[a]	Eval Prec
Surface Accuracy				
Precision	ANT0501, ANT0502	Errors in the aperture plane shall not exceed 320 μm RMS when operating in the Precision operating environment[b]	SYS1001, CAL0204	32 μm/ 70 cm
Normal	ANT0501, ANT0502	Errors in the aperture plane shall not exceed 600 μm RMS when operating in the Precision/Normal operating environment[b]	SYS1001, CAL0204	32 μm/ 70 cm

[a] See Dunbar (2020); Selina et al. (2018); Hales (2019).
[b] Note that the aperture plane error is approximately double the root sum square (RSS) of the surface error of the complete antenna optics system.

Radiometric holography measurements of the VLA antennas have been made for many years using strong continuum sources at X-, K-, and Q-band (Perley, 2021). Leveraging that experience, and the co-location of the ngVLA antenna at the VLA site, the default plan is to use interferometric holography to verify the surface performance of the ngVLA prototype antenna. An alternative system for measuring the ngVLA prototype antenna surface performance could be developed using a commercial laser tracker. We investigate this alternative measurement system in Section 6.2.1.

6.1 Radiometric Holography

Several measurement requirements drive the design of the ngVLA prototype holography measurement system:

- δd (cm): Resolution in the aperture plane
- θ_{ext} (deg): Holography map total extent
- Δt_{map} (hours): Total holography map time
- δz (μm): Surface deformation sensitivity

In the following we analyze each of these holography measurement drivers with a goal toward defining the holography measurement system. Figure 1 shows a sketch of two proposed holography map measurement scenarios. The star scanning pattern is preferred as it naturally allows for boresight measurements, required to track positioning stability during the holography measurement.

6.1.1 Resolution in the Aperture Plane δd

In order to be able to determine individual adjuster positioning to optimize antenna surface setting using holography measurements, one needs to be able to measure deformations over individual panels with enough resolution in the aperture to see the influence of individual panel adjusters. The panels of the ngVLA prototype antenna are 2.25 m by 2.13 m in size, with each panel having an adjuster near each panel corner and a fifth adjuster in the center of the panel. At this point we do not have a final design for the ngVLA prototype antenna panels, so we will assume that all panel adjusters are 0.13/2 m from any panel edge. This would imply that the minimum distance between any adjuster on a panel will be $\sqrt{2}$ m. Assuming a minimum of two holography measurement samples per adjuster, the minimum spatial sampling of the holography measurements will need to be $\frac{\sqrt{2}}{2}$ m, or about 70 cm. Figure 2 shows the relationship between a panel and the holography sampling of that panel.

[1] http://www.worldwidewords.org/weirdwords/ww-bou1.htm

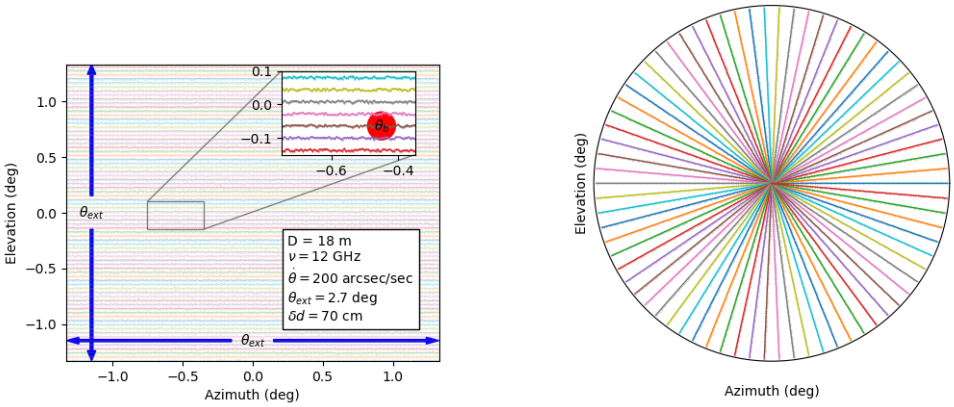

Figure 1: Sketches of two proposed ngVLA prototype antenna holography map measurement scenarios. Left: Boustrophedonic[1] scanning pattern for the measurement parameters listed inset. Right: Star scanning pattern for the same measurement parameters listed in the left panel inset. For both sketches, to simulate positioning jitter during scanning a 15 arcsec random wander has been assumed for these sketches, but the antenna should perform much better than this.

6.1.2 Holography Map Extent θ_{ext}

Using the equations presented in Baars et al. (2007) we can determine how our requirement for δd affects our measurement setup. Assuming a boustrophedonic[1] scanning pattern for the holography measurements, we can relate δd to the holography measurement parameters:

$$\begin{aligned} \delta d &= \frac{D}{N_{row}} \\ &= \frac{f_1 f_{apo} c}{\nu \theta_{ext}} \end{aligned} \tag{1}$$

where D is the antenna diameter, N_{row} is the number of rows in the holography map, f_1 is the primary beam taper factor ($f \simeq 1$), f_{apo} is an apodization smoothing factor used in the holography imaging to dampen ringing on the edge of the aperture (equal to 1.3; see Baars et al. (2007) for details), D is the antenna diameter, ν is the measurement frequency, and θ_{ext} is the angular extent of the holography map. Since all parameters in this equation are fixed except for ν and θ_{ext}, we solve Equation 1 for these two parameters:

$$\begin{aligned} \nu \theta_{ext} &= \frac{f_1 f_{apo} c}{\delta d} \\ &\simeq \frac{1.3 c}{70\,cm} \frac{GHz}{10^9} \frac{180\,deg}{\pi} \\ &\simeq 32\,\text{GHz deg} \end{aligned} \tag{2}$$

where we have assumed $\delta d = 70$ cm from Section 6.1.1. For Ku-band (12 GHz), $\theta_{ext} \simeq 2.7$ deg. Note that this value for θ_{ext} is similar to that commonly used for VLA holography (Perley, 2021).

6.1.3 Total Holography Map Time Δt_{map}

In order to assess the influence of varying meterological and antenna external heating influences (e.g. wind, solar illumination, ambient temperature changes, etc.), it will be necessary to acquire holography measurements within as short a period as possible. A holography measurement time of one hour is an attainable goal which will allow for the assessment of varying measurement conditions.

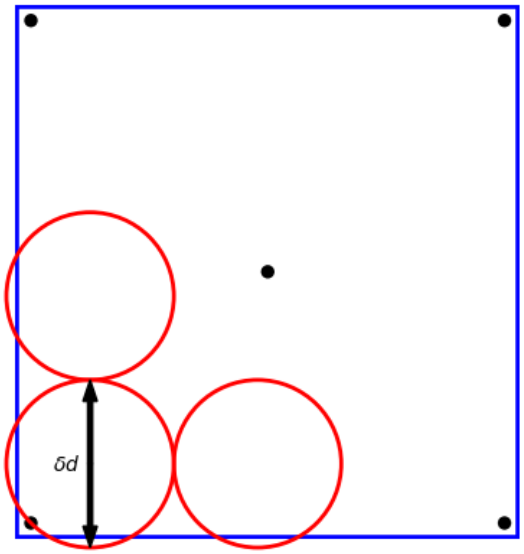

Figure 2: Sketch of the holographic sampling of a surface panel. The holography measurement sampling size δd is shown as red circles upon a schematic surface panel outlined in blue with black adjusters.

To quantify this goal in terms of our holography measurement parameters, we again refer to the equations presented in Baars et al. (2007):

$$\begin{aligned}
\Delta t_{map} &= N_{row} t_{row} \\
&= \frac{f_{osr}\theta_{ext}^2}{\dot{\theta}\theta_b} \\
&= \left(\frac{f_{osr}}{\nu\dot{\theta}}\right)\left(\frac{f_1 f_{apo} c}{\nu\delta d}\right)^2\left(\frac{\nu D}{f_1 c}\right) \\
&= \frac{c f_{osr} f_1 f_{apo}^2 D}{\nu\dot{\theta}(\delta d)^2} \\
&= \left(\frac{180\times 3600 c(cm/s)}{\pi 10^7}\right)\left(\frac{f_{osr} f_1 f_{apo}^2 D(m)}{\dot{\theta}(arcsec/sec)\nu(GHz)(\delta d(cm))^2}\right) \text{ seconds} \\
&\simeq \frac{171768 f_{osr} f_1 f_{apo}^2 D(m)}{\dot{\theta}(arcsec/sec)\nu(GHz)(\delta d(cm))^2} \text{ hours} \qquad (3)
\end{aligned}$$

For $f_{osr} = 2.2$, $f_1 = 1$, $f_{apo} = 1.3$, $D = 18\,\mathrm{m}$, $\dot{\theta} = 200\,\mathrm{arcsec/sec}$, $\nu = 12\,\mathrm{GHz}$, and $\delta d = 70\,\mathrm{cm}$, Δt_{map} is 0.98 hours. Note that the scanning rate chosen, 200 arcsec/sec, is significantly below the maximum tracking rate specification of 7.5 deg/min = 450 arcsec/sec.

6.1.4 Surface Deformation Sensitivity δz

In order to verify the surface accuracy performance of the ngVLA prototype antenna under normal and precision operating conditions, our holography measurements will need to have a measurement dynamic range of better than 5:1. This implies that our holography measurement system will need to have a surface deformation sensitivity (δz) of at least $160\,\mu\mathrm{m}/5 = 32\,\mu\mathrm{m}$.

From Perley (2021), Equations 21 through 23 and 29, the antenna equivalent flux density (S_a), the noise per sample in the aperture (σ) and the signal-to-noise ratio (SNR) in a holography map is

given by:

$$S_a = \frac{2kT_{sys}}{\eta_i \eta_b A_p} \tag{4}$$

$$\sigma = \frac{S_a}{2}\sqrt{\frac{N_{grid}}{Bt_{grid}}} \tag{5}$$

$$SNR = \frac{2S}{S_a}\sqrt{\frac{N_{ref} Bt_{grid}}{N_{grid}}} \tag{6}$$

$$= \frac{S\eta_i \eta_b \pi D^2}{4kT_{sys}}\sqrt{\frac{N_{ref} Bt_{grid}}{N_{grid}}} \tag{7}$$

where

- k is Boltzmann's constant,
- T_{sys} is the system temperature,
- η_i and η_b are the illumination and blockage efficiencies,
- A_p is the physical aperture of the antenna ($(\pi/4)D^2$),
- N_{grid} is the number of independent measurements in the final holography image[1],
- B is the detector bandwidth,
- t_{grid} is the integration time per final image grid point,
- S is the holography source flux,
- N_{ref} is the number of reference antennas used in the holography measurement.

We will need to know how many independent grid points we will have in our final holography image, and how much integration time we acquire at each of the independent grid positions. Those quantities are given by:

$$N_{grid} = \left(\frac{D}{\delta d}\right)^2 \tag{8}$$

$$t_{grid} = \frac{\Delta t_{map}}{N_{grid}}$$

$$= \frac{c f_{osr} f_1 f_{apo}^2}{\nu \dot{\theta} D}$$

$$= \left(\frac{180 \times 3600 c(m/s)}{\pi 10^9}\right)\left(\frac{f_{osr} f_1 f_{apo}^2 D(m)}{\dot{\theta}(arcsec/sec)\nu(GHz)(\delta d(cm))^2}\right) \text{ seconds} \tag{9}$$

$$\simeq \frac{6.2 \times 10^4 f_{osr} f_1 f_{apo}^2}{\dot{\theta}(arcsec/sec)\nu(GHz)D(m)} \text{ seconds} \tag{10}$$

where we have used Equation 3. For

- $D = 18\,\mathrm{m}$,
- $f_{osr} = 2.2$,
- $f_1 = 1$ (no taper),

[1]Note that $N_{grid} = N^2$ from Perley (2021).

- $f_{apo} = 1.3$,
- $\nu = 12\,\mathrm{GHz}$,
- $\dot{\theta} = 200\,\mathrm{arcsec/sec}$

$N_{grid} = 661$ (which is equivalent to a 26×26 square grid) and $t_{grid} = 5.3\,\mathrm{seconds}$.

In order to calculate the error in the holography measurement in terms of physical displacement, we note that the error in the illumination phase for the case with $SNR \gg 1$ is given by $\sigma_\phi = \frac{1}{SNR}$ (Perley, 2021). The error in the physical displacement of the surface is then given by

$$\delta z = \frac{\lambda}{4\pi SNR \cos\phi} \tag{11}$$

where ϕ is the tilt of the antenna surface relative to horizontal. Combining Equations 7 and 11

$$\begin{aligned} \delta z &= \left(\frac{c}{4\pi\nu\cos\phi}\right)\left(\frac{1}{2S}\sqrt{\frac{N_{grid}}{N_{ref}Bt_{grid}}}\right)\left(\frac{2kT_{sys}}{\eta_i\eta_b A_p}\right) \\ &= \frac{c\sqrt{N_{grid}}kT_{sys}}{\nu\pi^2 D^2 S\eta_i\eta_b\cos\phi\sqrt{N_{ref}Bt_{grid}}} \\ &\simeq \frac{6\times10^4\sqrt{N_{grid}}T_{sys}(K)}{\nu(GHz)D^2(m)S(Jy)\eta_i\eta_b\sqrt{N_{ref}B(MHz)t_{grid}(sec)}}\,\mu m \end{aligned} \tag{12}$$

where we have replaced λ with c/ν, A_p with $(\pi/4)D^2$, and assumed an average surface tilt angle (equivalent to the zenith angle) of 45 degrees (so that $\cos\phi = 1/\sqrt{2}$). For:

- $N_{grid} = 661$ (approximately 26×26),
- $D = 18\,\mathrm{m}$,
- $\epsilon_i = 0.978$,
- $\epsilon_b = 1$,
- $B = 1\,\mathrm{GHz}$,

Equation 12 becomes

$$\delta z \simeq \frac{154T_{sys}(K)}{\nu(GHz)S(Jy)\sqrt{N_{ref}t_{grid}(sec)}}\,\mu m \tag{13}$$

Table 5 lists sources from the VLA Calibrator Catalog (Sjouwerman, 2021) with flux greater than 5 Jy, suggesting that a sufficient number of sources with fluxes of several Jy are available at X- and Q-band from the VLA site. Figure 4 shows the (Az,El) distribution of these sources on 2021-05-01. Figure 3 shows Equation 13 plotted as a function of frequency and number of reference antennas for three holography grid point integration times and holography target source fluxes. Checking this result, we note that for the Q-band holography system described in Perley (2021), the quantities in Equation 12 are:

- $N_{grid} = 1849$ (43×43),
- $T_{sys} = 150\,\mathrm{K}$,
- $\nu = 43\,\mathrm{GHz}$,
- $D = 25\,\mathrm{m}$,
- $\epsilon_i\epsilon_b = 0.85$,

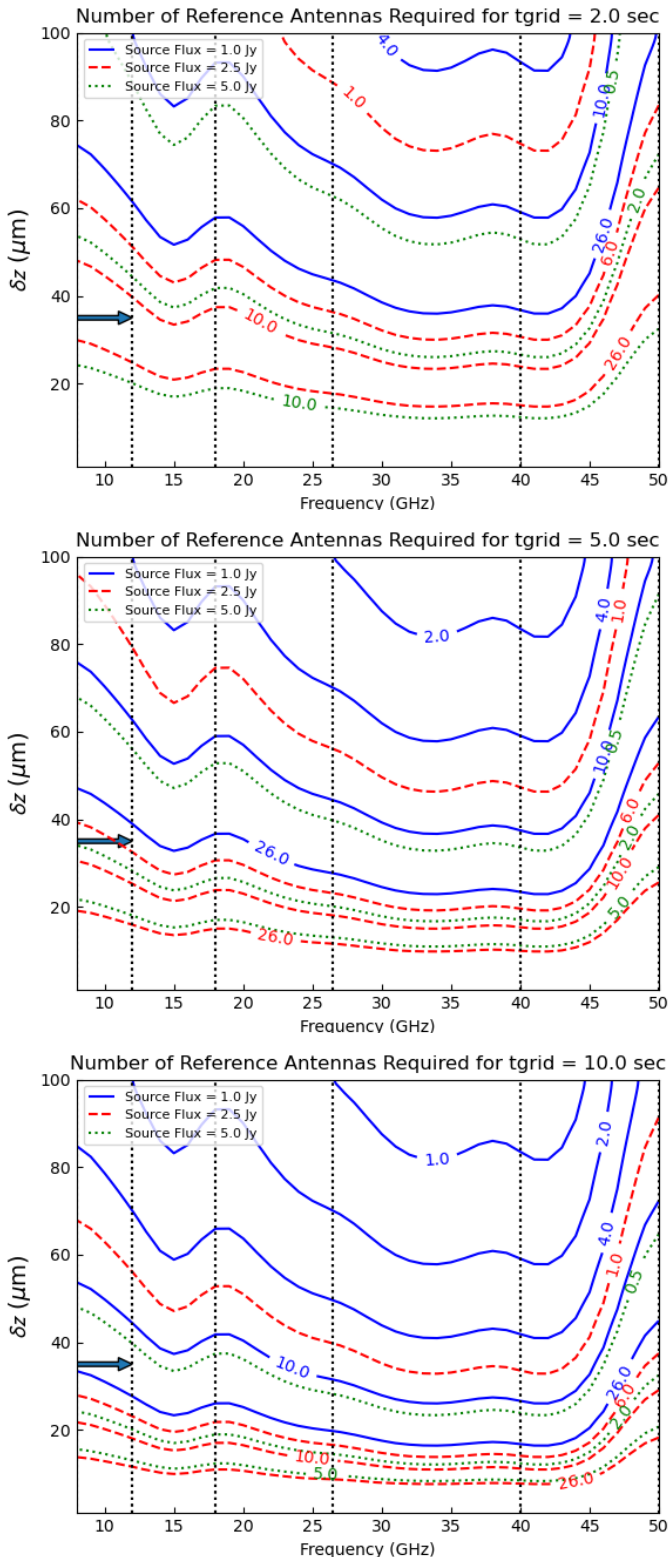

Figure 3: Equation 13 as a function of frequency. Contours are number of reference antennas for three different holography grid point integration times (t_{grid}) and holography target source fluxes (S). VLA receiver zenith system temperatures have been taken from the XML file which feeds the ETC. Vertical black dotted lines mark receiver band edges. A black arrow indicates the holography measurement sensitivity target of 35 μm.

- $B = 128\,\mathrm{MHz}$,
- $t_{grid} = 10\,\mathrm{sec}$

so that the equation for δz becomes:

$$\delta z = \frac{557}{S(Jy)\sqrt{N_{ref}}}\,\mu m \tag{14}$$

For a 10 Jy target and $N_{ref} = 13$, $\delta z \simeq 15\,\mu$m.

Table 5: VLA Calibrator Catalog Sources with Flux ≥ 5 Jy

Source	X-/Q-band Flux (Jy)	Transit Elevation (deg)
J0319+4130	21.7/9.0	82
J0359+5057	5.1/5.5	72
J0555+3948	6.2/...	72
J0609−1542	9.2/6.2	39
J0927+3902	7.2/...	84
J1229+0203	27.5/13.5	56
J1230+1223	.../12.0	68
J1256−0547	15.6/24.7	48
J1331+3030	5.23/...	85
J1337−1257	.../7.0	42
J1642+3948	7.0/11.2	83
J1733−1304	10.5/9.0	42
J1743−0350	.../5.1	51
J1833−2103	6.75/...	33
J1924−2914	5.8/9.1	26
J2136+0041	7.03/...	56
J2148+0657	6.6/7.6	62
J2225−0457	5.6/...	50
J2253+1608	10.9/17.1	72

Summarizing the analysis of the holography measurement sensitivity shown in Figure 3 and 4 and Table 5, holography measurements that meet our sensitivity requirement of 35 μm:

- Are possible at X-band, but only for:
  - A longer grid point integration time ($\gtrsim 10\,\mathrm{sec}$) and a large number of reference antennas ($\gtrsim 20$) when weaker target sources ($\sim 1\,\mathrm{Jy}$) are used.
  - A reasonable grid point integration time of 5 sec and number of reference antennas ($\lesssim 7$) when stronger target sources ($\gtrsim 2.5\,\mathrm{Jy}$) are used.
- Are possible at the low frequency end of Q-band for target sources with flux $\gtrsim 2.5$ Jy, grid point integration times $\gtrsim 2$ sec, and no more than ~ 5 reference antennas.

Table 6 summarizes the measurement parameters for a typical holography map.

Table 6: Holography Map Parameter Summary

N_{grid}	B (GHz)	ν (GHz)	$\dot{\theta}$ (arcsec/sec)	t_{grid} (sec)	Δt_{map} (min)	θ_{ext} (deg)
661	1	12	200	5.3	60	2.7
661	1	43	100	3.0	120	0.7

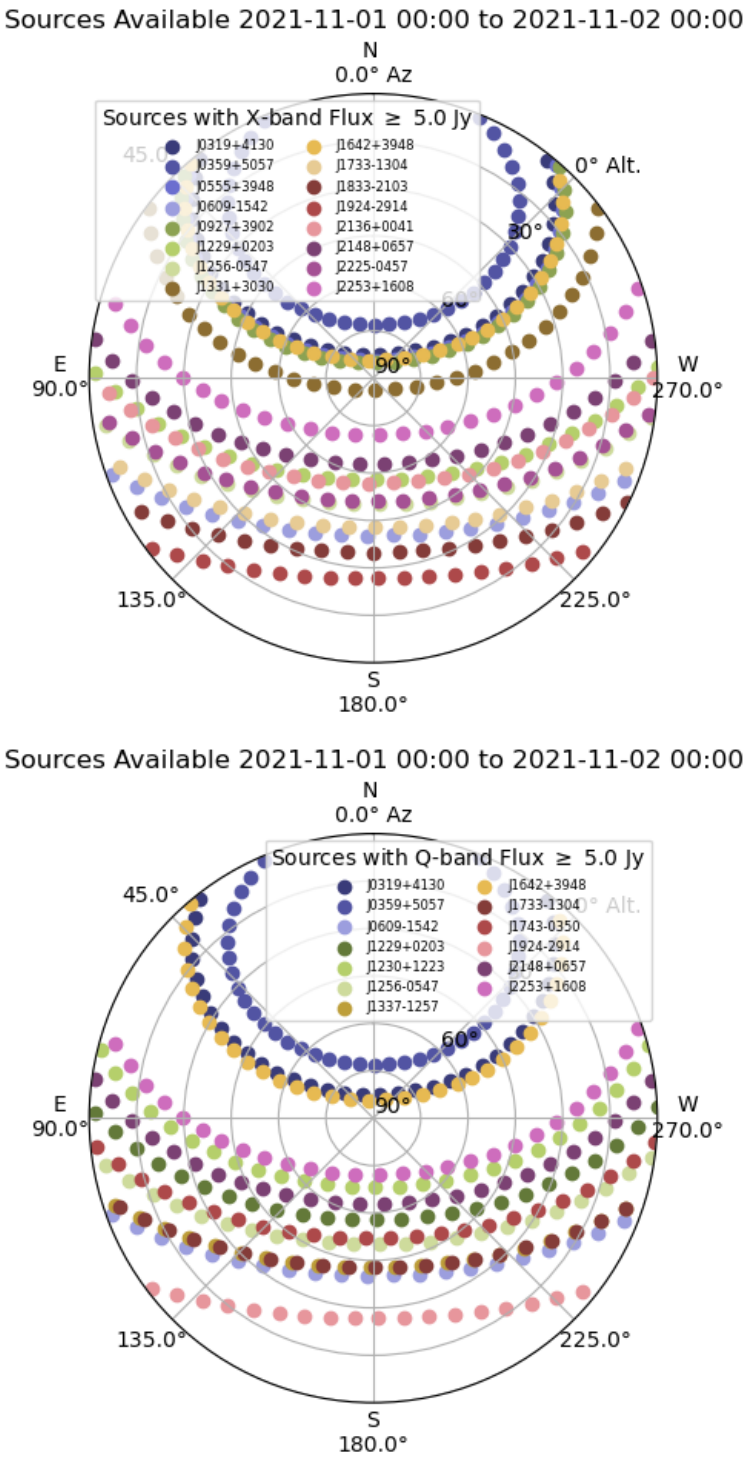

Figure 4: (Az,El) distribution of sources with X-band (top) and Q-band (top) flux greater than or equal to 5 Jy on a typical day.

6.1.5 Communication Satellites as Holography Signal Sources

Geosynchronous and geostationary satellites have been used as holography sources for successfully measuring and setting radio telescope primary reflectors with total RMS surface accuracies as low as 12 μm (Submillimeter Telescope Observatory (SMT); Baars et al., 1999). The NRAO 12 m (using the geosynchronous Lincoln Experimental Satellite numbers 8 and 9 at 38 and 39 GHz, respectively; Mayer et al., 1994) and the Green Bank Telescope (using the geostationary Galaxy 28 satellite beacon at 11.701 GHz; Hunter et al., 2011) both used communications satellites as holography sources to set their primary reflector surfaces. Tracking of communications satellites is relatively straightforward given the availability of NORAD two-line element (TLE) sets which describe the Keplerian orbital elements of a satellite, redistributed and supplemented by CelesTrak[2]. Communications satellites may offer access to very strong holography target sources at a variety of elevation angles which can be used for ngVLA prototype antenna surface verification. One can use either the beacon CW tones (with a suitable narrow band filter in the backend) or the broadband (tens to hundreds of MHz) signals with digital TV content (using matched-length IF cables and a continuum correlator). Note that geostationary satellites orbit at a height above the Earth's surface of 35,786 km, which is about 44,000 km from the surface at latitude=40 deg and is well beyond the far-field distance of $R_{ff} = 2D^2/\lambda \simeq 65/\lambda(cm)km$. Thus, all signals from a geostationary satellite arrive at the ngVLA antenna as a plane wave.

6.2 Alternative Surface Accuracy Verification Methods

In the following we investigate alternative methods for verifying the ngVLA prototype antenna primary reflector surface accuracy. Table 7 compares all surface measurement techniques derived from this assessment.

Table 7: Antenna Surface Measurement System Comparison

System	Meas Time (min)	δd (cm)	Δz (μm)
TLS/LASSI	~ 2	$\sim 6^a$	100 ± 30
OOF	~ 15	~ 500	$\sim \frac{\lambda}{100}$
Interferometric Holography	~ 60	~ 70	~ 10

[a] For a distance of 100 m.

6.2.1 Terrestrial Laser Scanner Antenna Surface Measurement

Relatively recent improvements in the measurement precision of Terrestrial Laser Scanners (TLSs) have allowed for their use in measuring the surfaces of large antennas, including the Effelsberg 100 m (Leica ScanStation P20; Holst et al., 2015) and GBT (Leica ScanStation P40 within the LASSI system; Salas et al., 2020, see Figure 5). Primary surface measurements using the Leica TLS systems noted can make surface measurements over the full elevation range of an antenna in a matter of minutes when properly mounted so as to allow full-view of the antenna primary aperture. Unfortunately, a TLS alone has a surface accuracy measurement precision of only 1.5 to 2.0 mm RMS (Holst et al., 2015). One can improve on the accuracy of a TLS measurement by using a suitable reference measurement to remove systematics introduced by the TLS itself. The Laser Antenna Surface Scanning Instrument (LASSI) developed for the GBT (Salas et al., 2020) is such a system, with a reported measurement uncertainty of $\epsilon_{LASSI} = 100 \pm 30\,\mu$m. The "point cloud" of distance measurements from this system contains approximately twenty million individual measurements, offering substantial spatial resolution on the primary surface. Unfortunately, it appears that the accuracy of these TLS-based measurement systems is not able to meet the requirements for verifying the ngVLA prototype antenna surface accuracy requirement.

[2]See http://celestrak.com/NORAD/elements/supplemental.

Figure 5: The Leica ScanStation P40 Terrestrial Laser Scanner.

6.2.2 Out-of-Focus (OOF) Holography

The Out-of-Focus (OOF) holography technique has been used for decades to provide a relatively simple measurement of the large-scale deformations on an antenna's primary aperture. For example, the GBT (Nikolic et al., 2007b,a) has used OOF measurements at 43 GHz for many years to regularly measure and correct its active surface so as to provide optimized performance for observing frequencies above 20 GHz. The OOF technique entails making total power continuum images of the antenna primary beam using a strong astronomical (preferably) point source both in- and out-of-focus. A typical measurement time for an OOF set is $\sim$ 15 minutes and utilizes the facility continuum detectors, thus requiring no special hardware. The primary beam measurements are then fit to a model which parameterizes the possible aberrations due to defocus as a linear combination of Zernike polynomials. The magnitudes of the Zernike coefficients are used to infer the surface accuracy of the primary reflector under measurement. Figure 6 is an example of an OOF measurement from the GBT.

As is apparent from Figure 6, OOF holography is only sensitive to wavefront errors which are correlated over large scales in the aperture plane. For an 18 m aperture this resolution scale size is about 5 m. Furthermore, the accuracy of this measurement technique is $\sim \lambda/100$ (Nikolic et al., 2007a). It appears that the accuracy and resolution of the OOF holography technique is not able to meet the requirements for verifying the ngVLA prototype antenna surface accuracy requirement.

6.3 Aperture Efficiency Measurement

As the aperture efficiency is the most direct way to verify the surface accuracy of an antenna, using aperture efficiency measurements toward a well-calibrated source can provide constraints on the underlying quality of an antenna's surface. Following the formalism described in Mangum (2017) we can

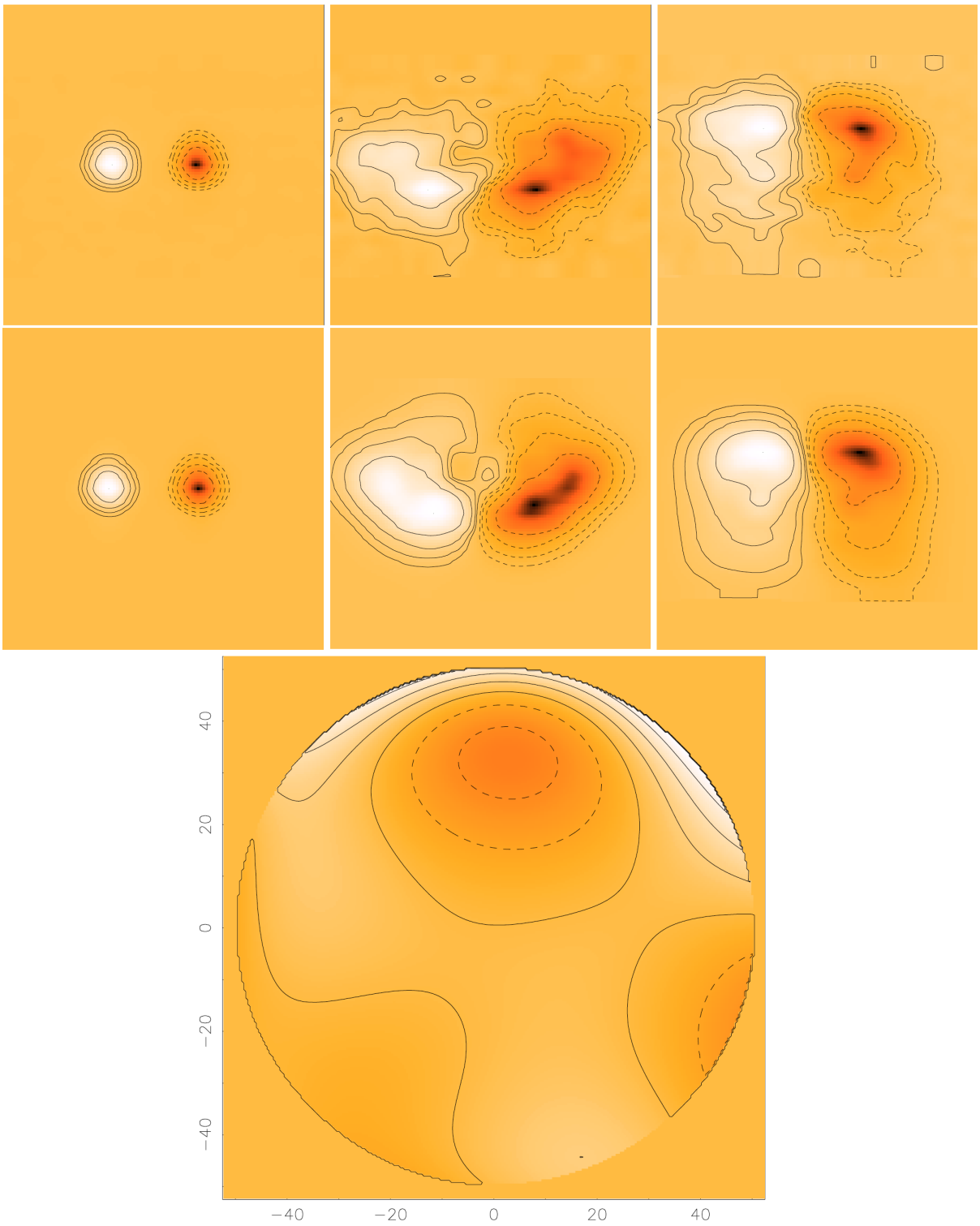

Figure 6: Sample GBT 43 GHz OOF measurements from Nikolic et al. (2007a). Top Panel: In- and $\pm 5\lambda$-out-of-focus (left-to-right) continuum images of 3C 279. The top row in this panel shows the actual measurements, while the bottom row shows the simulated beam maps of the best-fitting model (using Zernike polynomials up to fifth radial order inclusive) to the observed maps in the top row. An area of $210'' \times 210''$ has been imaged in (Az,El). Bottom Panel: Measured and calibrated wavefront error distribution for a 43 GHz GBT OOF measurement. The weighted RMS is $\sim 220\,\mu$m in this image. The grayscale range in this diagram is ± 2 radians, and the contours are at half-radian intervals.

write the aperture efficiency in terms of other signal reception efficiencies as follows:

$$\begin{aligned}
\eta_A &\equiv \frac{A_{max}}{A_g} \\
&\equiv \eta_i \eta_s \eta_r \eta_p \eta_e \eta_f \eta_b \\
&= \eta_i \eta_s \eta_r \eta_p \eta_f \left\{ \exp\left[-\left(\frac{4\pi\sigma}{\lambda} \right)^2 \right] + \frac{1}{\eta_{A0}} \left(\frac{c}{D} \right)^2 \left\{ 1 - \exp\left[-\left(\frac{4\pi\sigma}{\lambda} \right)^2 \right] \right\} \right\} \left(1 - \frac{A_b}{A_r} \right)^2 \\
&\simeq \eta_i \eta_s \eta_r \eta_p \eta_f \exp\left[-\left(\frac{4\pi\sigma}{\lambda} \right)^2 \right] \left(1 - \frac{A_b}{A_r} \right)^2
\end{aligned} \tag{15}$$

where in the last step we assume that the correlation length of the surface errors are small in comparison to the diameter of the antenna ($c \ll D$) and define:

- η_i is the illumination efficiency (0.97; EMSS, 2019),
- η_s is the spillover efficiency, which is a measure of the fraction of the radiated power from the antenna feed that spills-over the edge of the subreflector onto cold sky (for cassegrain focus optics) or the edge of the main reflector onto warm ground (for prime focus optics). For ngVLA the spillover efficiencies are 0.83 at 2 and 6 GHz and 0.92 at all other frequencies.
- η_r is the radiation efficiency (ohmic loss),
- η_p is the polarization efficiency, which is a measure of the loss due to cross-polarized signal, is assumed to be 1.0 for ngVLA,
- η_e is the surface error efficiency, normally defined using the Ruze (1966) formula,
- η_f is the focus efficiency. Displacements of the feed parallel (X and Y) or axial (Z) to the aperture plane result is large-scale phase errors over the aperture. Normally these errors are minimized by regular adjustment and optimization of the antenna focus. For ngVLA, the focus efficiencies are estimated to be 1.0 at 2.0, 6.0, and 10.0 GHz and 0.99, 0.99, 0.97, 0.96, and 0.94 at 30, 50, 80, 100, and 120 GHz, respectively.
- η_b is the blocking efficiency, which characterizes the efficiency degradation due to physical structures (and gaps) lying between the source and the reflecting surface. These blockage structures are generally split into two types: those that block the plane wave from the source and those that block the spherical wave propagating from the reflector surface. As the ngVLA antennas have an unblocked aperture, $\eta_b = 1$.

In Figure 7 we show the ngVLA 18 m antenna surface efficiency as a function of wavelength. Red and blue lines mark the $\sigma = 160\,\mu$m (precision) and $300\,\mu$m (normal) surface accuracy requirements. As is apparent, at X-band ($\lambda = 25 - 75$ mm) the surface efficiency, and therefore the aperture efficiency, changes by only a few percent when σ changes by even 100's of microns. At Q-band ($\lambda = 7$ mm), the situation is a bit more promising, with η_e ranging from 0.93 at $\sigma = 160\,\mu$m to 0.75 at $\sigma = 300\,\mu$m. Using a flux calibrator whose flux is known to better than $\sim 5\%$, aperture efficiency measurements at Q-band should be able to at least verify the surface accuracy performance under normal conditions, and perhaps even under precision conditions (barely).

7 Pointing Requirement

In the following we describe the measurement systems and techniques which we believe will allow for the proper characterization of the ngVLA 18 m antenna pointing performance. Table 8 lists these antenna performance requirements and the requirements for the associated measurement systems that NRAO will need to develop.

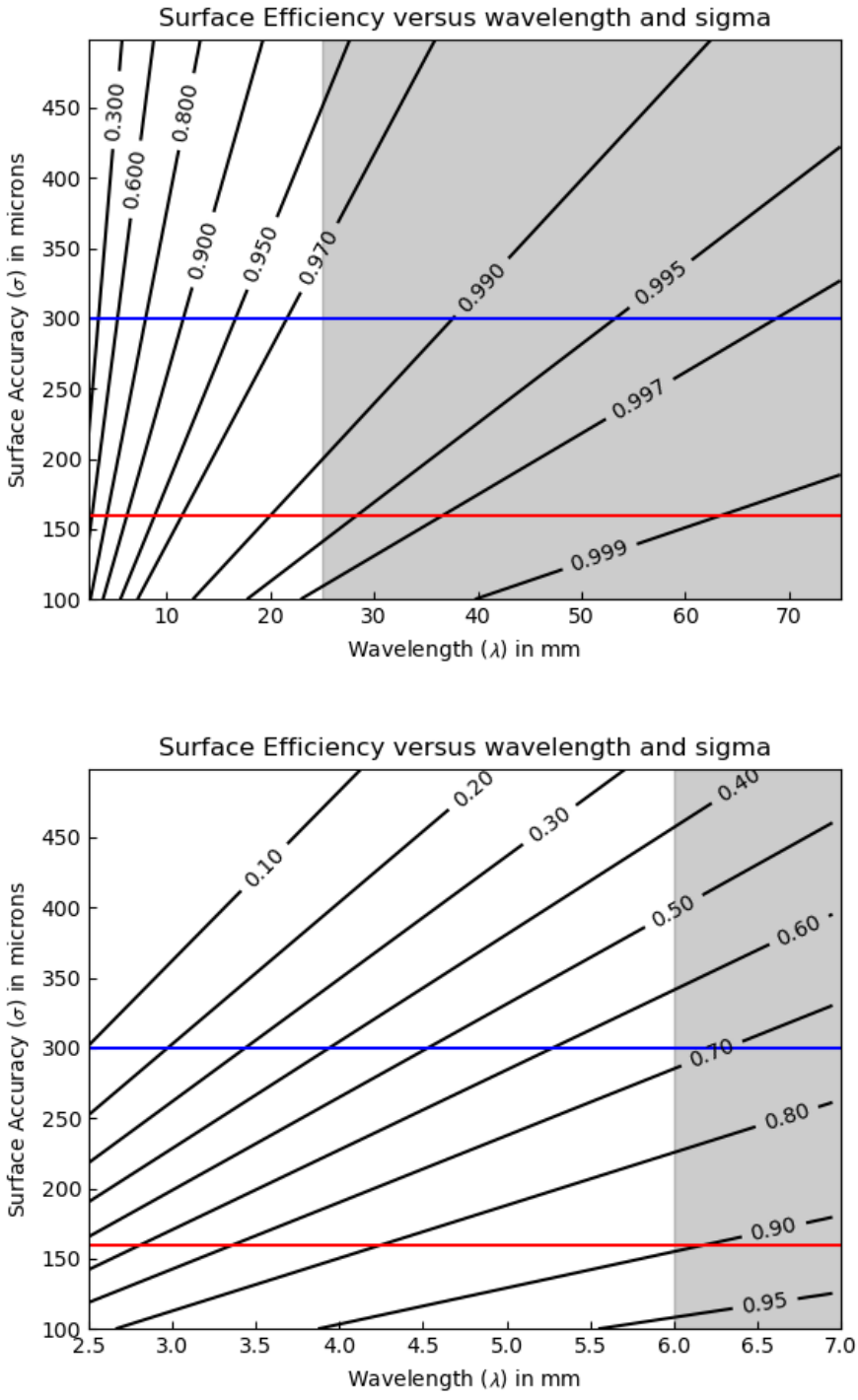

Figure 7: Surface efficiency as a function of wavelength. Red (precision) and blue (normal) horizontal lines indicate the required surface accuracy under their respective conditions. Top panel scaling from $\lambda = 2.5$ to 75 mm with shading showing X-band. Bottom panel runs from $\lambda = 2.5$ to 7 mm with shading showing Q-band.

Table 8: ngVLA 18 m Antenna Pointing Requirements

Op Env	Req #[a]	Value	Trace[a]	Eval Prec
Absolute Pointing Error				
Precision	ANT0611	18″ RMS. Goal of 15″ RMS.	CAL0201	5″
Normal	ANT0621	30″ RMS. Goal of 25″ RMS.	CAL0201	8″
Referenced Pointing Error				
Precision	ANT0612	3″ RMS within 3° of the target position and 15 minutes of time	CAL0201	1″
Normal	ANT0622	5″ RMS within 3° of the target position and 15 minutes of time	CAL0201	1″

[a] See Dunbar (2020); Selina et al. (2018); Hales (2019).

Radiometric pointing has been used for decades to characterize and track the pointing performance of radiometric antennas. On radiometric interferometers, higher signal-to-noise is gained when performing pointing using multiple antennas simultaneously. As this technique is well-established, and represents the method used to monitor pointing performance and stability during ngVLA operations, interferometric pointing will be the default technique used to characterize the ngVLA prototype antenna's pointing performance. In the following section we describe how this measurement system will work and characterize its sensitivity assuming the ngVLA prototype radiometer system described in Section 6.1. In Section 7.2 we consider alternative pointing measurement systems, for completeness.

7.1 Interferometric Pointing

Since the radiometric primary beam full-width at half-maximum (FWHM) is a fundamental parameter to which the sensitivity of various radiometric pointing measurement systems need to be compared, we start with a calculation of this parameter for all ngVLA observing bands. The general equation for primary beam FWHM θ_B is given by:

$$\theta_B = b\lambda/D \tag{16}$$

where b accounts for any taper applied to the illumination. Since the ngVLA antenna aperture is defined to have an illumination efficiency of 0.978 at all frequencies, for an assumed quadratic illumination function we can calculate the scaling factor b for the ngVLA antennas. As noted in Mangum (2017) the illumination efficiency is a measure of how well the illumination function samples the aperture of the antenna and is defined as follows (Silver, 1949):

$$\eta_i \equiv \frac{\left[\int F(r,\phi)dA\right]^2}{\int F^2(r,\phi)dA} \tag{17}$$

where $F(r,\phi)$ is the illumination function and the integration is carried out over the antenna aperture A. For a circularly-symmetric aperture the integration over ϕ is unity, leaving the radial dependence as the important factor in $F(r,\phi) = F(r)$. Two convenient and often-used forms for $F(r)$; a gaussian distribution with edge taper T_e (in dB):

$$F(r)_{gauss} = \exp\left(-\alpha r^2\right) \tag{18}$$

where $\alpha \equiv (T_e/20)\ln(10)$, and a quadratic on a pedestal distribution:

$$\begin{aligned} F(r)_{quadratic} &= \tau + (1-\tau)\left(1-r^2\right) \\ &= 1-(1-\tau)\,r^2 \end{aligned} \tag{19}$$

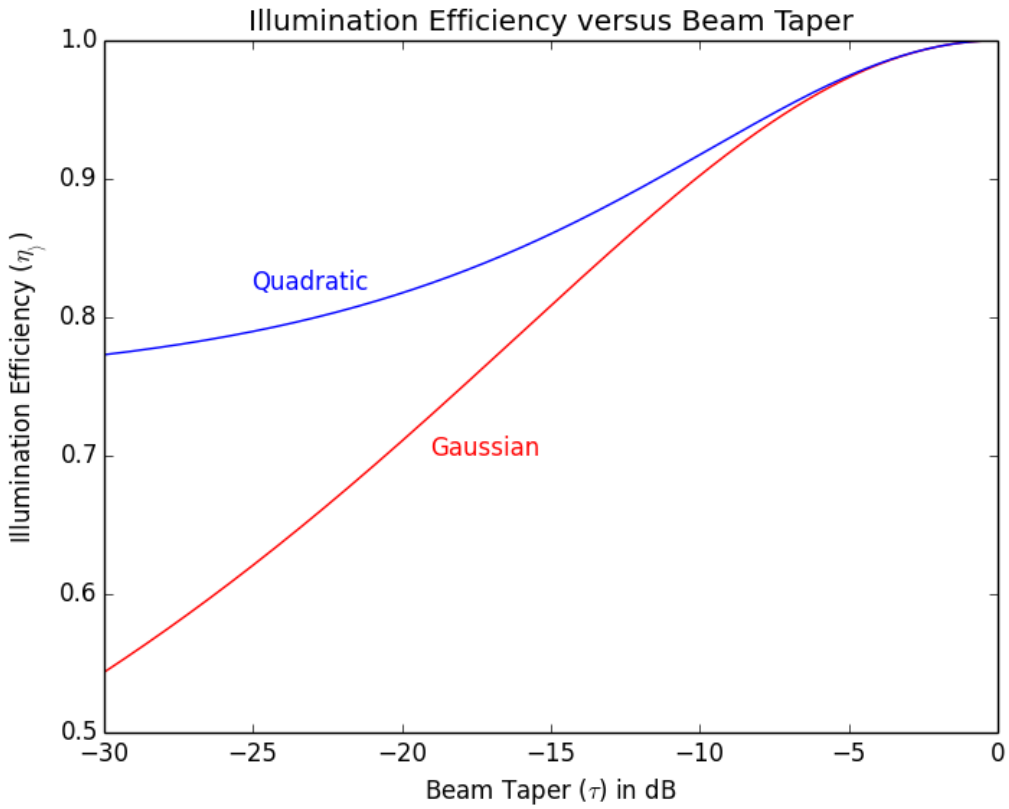

Figure 8: The illumination efficiency (η_i) for the gaussian (red) and quadratic (blue) taper functions (Equations 20).

where $\log(\tau) = T_e/20$. In both equations r is the normalized aperture radius. Inserting Equations 18 and 19 into Equation 17 results in the following expressions for η_i:

$$\begin{aligned} \eta_i^{gaussian} &= \frac{2\left(1-\exp -\alpha\right)^2}{\alpha\left(1-\exp -2\alpha\right)} \\ \eta_i^{quadratic} &= \frac{3\left(1+\tau\right)^2}{4\left(1+\tau+\tau^2\right)} \end{aligned} \tag{20}$$

Figure 8 shows Equations 20 for representative values of the beam taper T_e.

The normalization factor which relates the beam taper τ to the scaling factor b in the equation for the primary beam FWHM (θ_B; Equation 16) is given by (see Equation 4.13 in Baars et al. (2007), (which is quoted to be accurate over the range −20 to 0 dB)

$$b = 1.269 - 0.566\tau + 0.534\tau^2 - 0.208\tau^3 \tag{21}$$

A spline fit to the FWHM values as a function of the beam taper τ for $\tau = -30$ to 0 dB indicates that

$$b = (1.266 \pm 0.0001) - (0.568 \pm 0.002)\,\tau + (0.536 \pm 0.004)\,\tau^2 - (0.208 \pm 0.003)\,\tau^3 \tag{22}$$

Figure 9 shows Equations 21 and 22 as functions of the beam taper τ.

Using the quadratic form for the illumination function (Equation 20) with our known illumination efficiency of 0.978 and the form for b as a function of the illumination taper τ given by Equation 21,

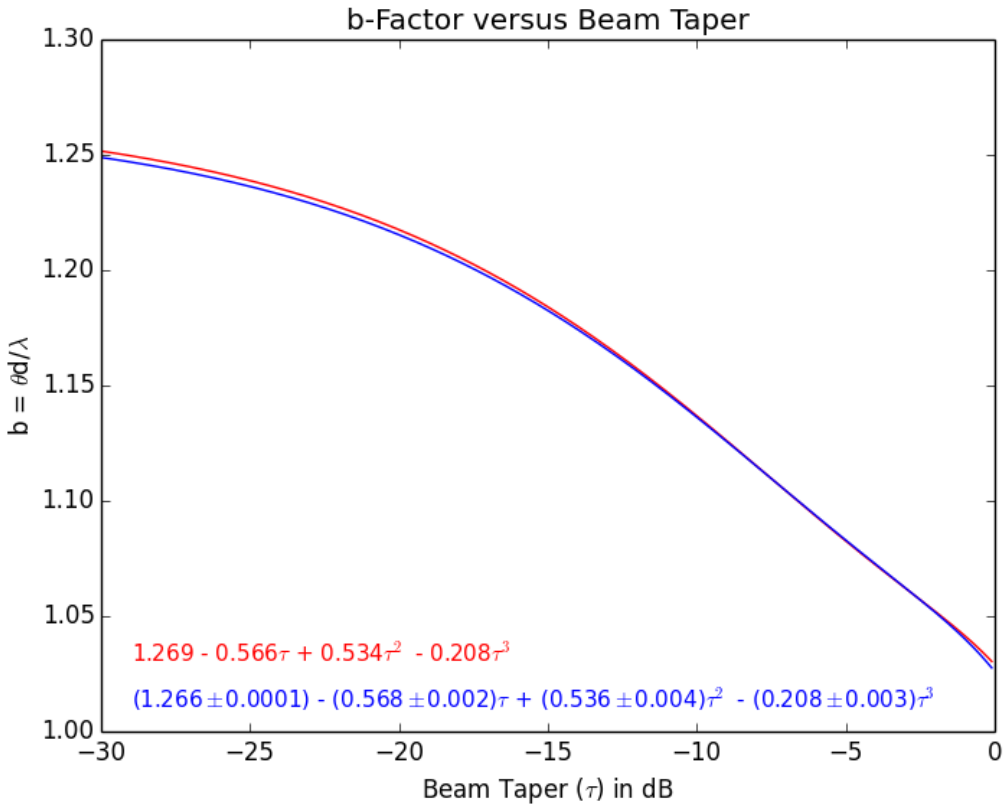

Figure 9: The scaling factor b in the expression for the antenna beam HPBW (Equation 16) as a function of the beam taper for the quadratic taper function (Equations 20), given by Equation 21 (from Baars et al., 2007, Equation 4.13), shown in red, and derived from a spline fit to the FWHM values as a function of the beam taper τ (blue), with parameter uncertainties.

we can solve the resulting quadratic equation for τ as a function of b. This calculation yields a beam taper τ of -5.3 dB and $b = 1.08$. The ngVLA primary beam size is then given by:

$$\begin{aligned} \theta_B &= \frac{1.08\lambda}{D}\ radians \\ &\simeq \frac{3710}{\nu(GHz)}\ arcsec \end{aligned} \tag{23}$$

Table 9 lists beam sizes for the lower and upper end of each ngVLA receiver band.

Table 9: ngVLA 18 m Antenna Primary Beam Sizes

Receiver Band	Frequency Range (GHz)	θ_B Range (arcsec)
Band 1	1.2–3.5	3091.7–1060.0
Band 2	3.5–12.3	1060.0–301.6
Band 3	12.3–20.5	301.6–181.0
Band 4	20.5–34.0	181.0–109.1
Band 5	30.5–50.5	121.6–73.5
Band 6	70.0–116.0	53.0–32.0

Radiometric pointing uses the same basic measurement system as that used to perform interferometric holography (Section 6.1). Starting from the radiometric total power sensitivity equations presented in Section 6.1.4 (Equations 7), we set $N_{grid} = 1$ so as to obtain the single-position signal-to-noise ratio (SNR):

$$S_a = \frac{2kT_{sys}}{\eta_i\eta_b A_p} \tag{24}$$

$$\sigma = \frac{S_a}{2\sqrt{Bt_{point}}} \tag{25}$$

$$SNR = \frac{2S}{S_a}\sqrt{N_{ref}Bt_{point}} \tag{26}$$

$$= \frac{S\eta_i\eta_b\pi D^2\sqrt{N_{ref}Bt_{point}}}{4kT_{sys}} \tag{27}$$

$$\simeq 180.3\frac{S(Jy)\sqrt{N_{ref}B(MHz)t_{point}(sec)}}{T_{sys}(K)} \tag{28}$$

where t_{point} is the integration time per position during a total power pointing measurement, $\eta_i = 0.978$, $\eta_b = 1.0$, and $D = 18$ m (see Section 6.1.4). As we need to be sensitive to reference pointing errors of 1 arcsec, and assuming that we can determine the peak of a gaussian source to an accuracy of $\theta_{point} = \theta_B/SNR$, we can combine Equations 23 and 28:

$$\begin{aligned} \frac{\theta_B}{SNR} &\simeq \frac{20.57T_{sys}(K)}{\nu(GHz)S(Jy)}\frac{1}{\sqrt{N_{ref}B(MHz)t_{point}(sec)}} \equiv \theta_{point} \\ S^2(Jy)\theta^2_{point}N_{ref}t_{point}(sec) &= \frac{423.2}{B(MHz)}\left(\frac{T_{sys}(K)}{\nu(GHz)}\right)^2 \end{aligned} \tag{29}$$

A general calculation of the N_{ref} requirements as a function of frequency, θ_{point}, t_{point}, S, and using a realistic distribution of T_{sys} (Figure 10) as a function of frequency is shown in Figure 11. The general conclusions one can draw from Figure 11 is that, assuming a pointing measurement integration time of 5 seconds:

- The 30 arcsec normal absolute pointing error requirement, which requires a 8 arcsec pointing precision, can be evaluated at X- or Ku-band with no more than 2 or 1 reference antennas, respectively, assuming sufficient pointing sources with fluxes of 100 mJy or larger are available. An analysis of the VLA calibrator catalog (Sjouwerman, 2021) indicates that there are 903 point sources with fluxes ≥ 200 mJy at X-band.

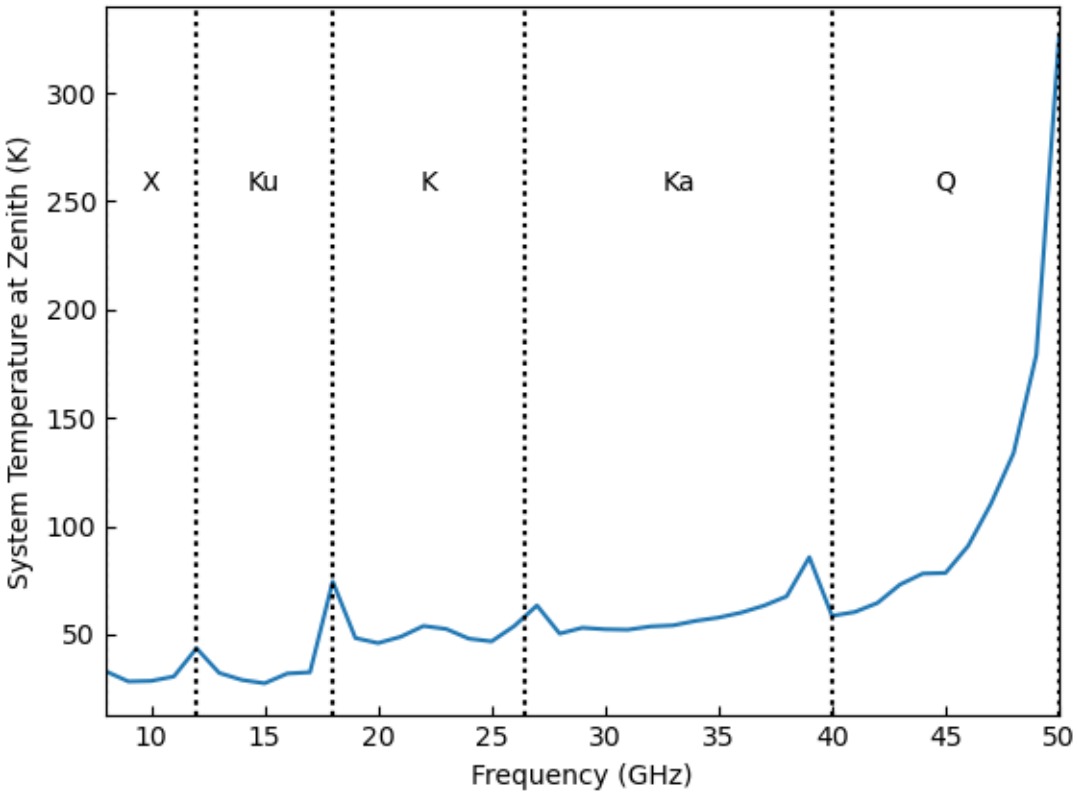

Figure 10: VLA system temperature at zenith as a function of frequency. Receiver bands and band edges are marked. Values are derived from the XML file used to drive the VLA exposure time calculator (ETC).

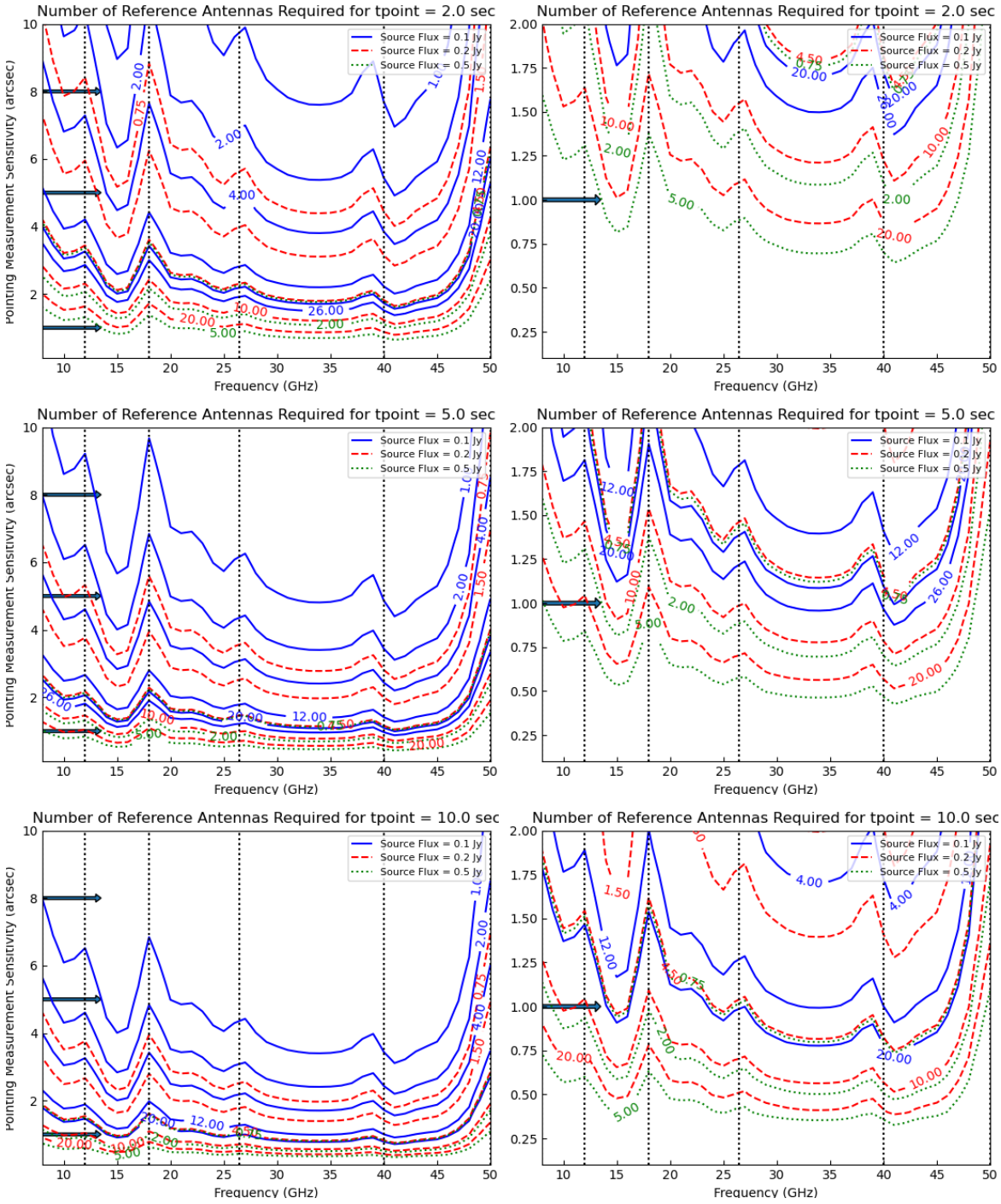

Figure 11: N_{ref} as a function of the observing frequency and required pointing sensitivity (θ_{point}) for three different pointing measurement integration times (t_{point}). VLA receiver zenith system temperatures have been taken from the XML file which feeds the ETC. Left panels show N_{ref} over the full range of pointing measurement sensitivity (see Table 8), while the panels on the right are zoomed to a maximum of $\theta_{point} = 2$ arcsec. Vertical black dotted lines mark receiver band edges, while black arrows indicate pointing measurement sensitivity requirements (see Table 8). Nonsensical contour levels (i.e. 0.75) used to improve contour visibility.

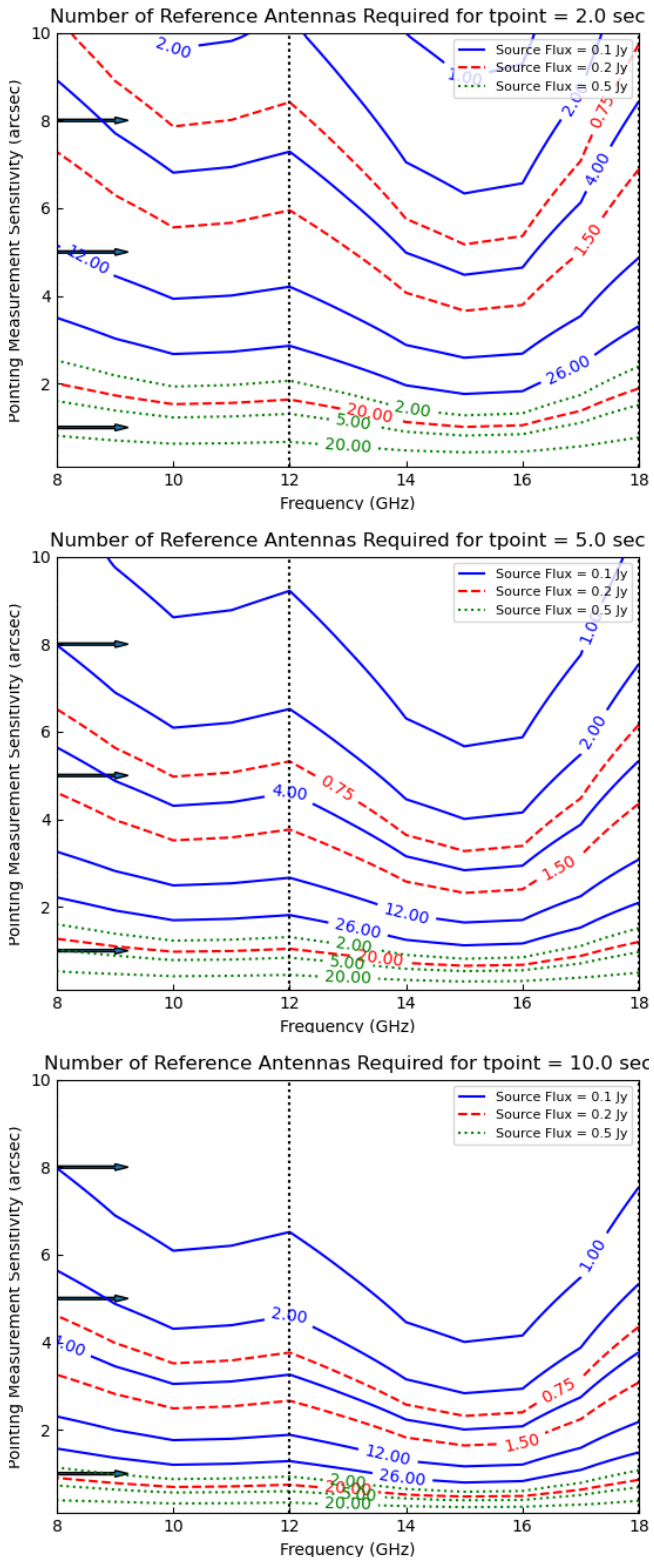

Figure 12: Same as Figure 11, but showing only X- and Ku-band. N_{ref} as a function of the observing frequency and required pointing sensitivity (θ_{point}) for three different pointing measurement integration times (t_{point}). VLA receiver zenith system temperatures have been taken from the XML file which feeds the ETC. Vertical black dotted lines mark receiver band edges, while black arrows indicate pointing measurement sensitivity requirements (see Table 8). Nonsensical contour levels (i.e. 0.75) used to improve contour visibility.

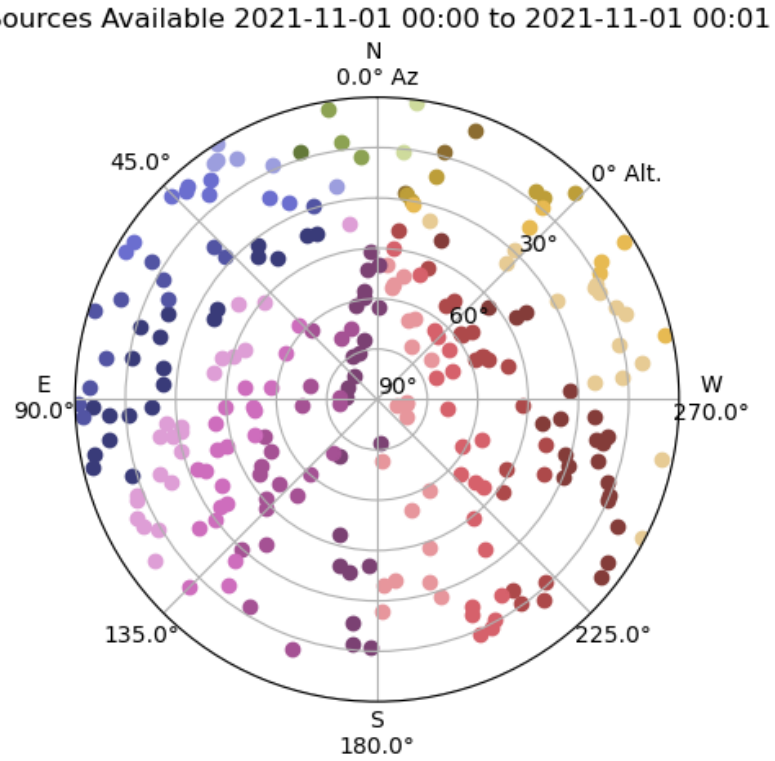

Figure 13: Distribution of Q-band point sources with fluxes ≥ 500 mJy from the VLA calibrator catalog for a randomly-chosen time. There are a total of 426 Q-band point sources shown.

- The 18 arcsec precision absolute pointing error requirement, which requires a 5 arcsec pointing precision, can be evaluated at X- or Ku-band with no more than 4 or 3 reference antennas, assuming sufficient pointing sources with fluxes of 100 mJy or larger are available.
- The 3 and 5 arcsec precision and normal referenced pointing error requirement, both of which require a 1 arcsec pointing precision[3], can only be evaluated at a high-frequency receiver band given the prohibitively large number of reference antennas ($\gtrsim 27$) required for X- or Ku-band measurements with 100 mJy sources. For the middle of Ka-band or the low-end of Q-band, no more than 8 reference antennas are required, assuming sufficient pointing sources with fluxes of 200 mJy or larger are available. If stronger sources are used, the maximum number of reference antennas required drops to 2 if sources with fluxes of 500 mJy or larger are used. An analysis of the VLA calibrator catalog (Sjouwerman, 2021) indicates that there are 426 point sources with fluxes ≥ 200 mJy at Q-band (Figure 13).
- Note that the system temperatures used are for measurements at the zenith. A more realistic calculation would include a zenith angle correction, which should affect Q- and K-bands more significantly than the others (Butler, 2002).
- Site atmospheric availability for observations at X- and Q-band (`https://science.nrao.edu/facilities/vla/proposing/VLA-API-wind/monthly-conditions-at-the-vla`) indicates that one can do X-band measurements year-round at any LST. Q-band atmospheric availability is much more variable, with winter availability generally 20% to 80% of the time, dropping to 5% to 70% during the rest of the year, with significant variation as a function of LST.

[3]We have relaxed the normal 5σ sensitivity limit to 3σ as sub-arcsec pointing precision measurements will very difficult to attain.

7.2 Alternative Pointing Systems

Optical Pointing Telescopes (OPTs) have been used extensively on radio telescopes to both characterize and monitor pointing performance on both prototype and production antennas (Mangum et al., 2006). For two main reasons:

- The development of an OPT for ngVLA requires a significant engineering effort, both for the design of the OPT and for its mounting on the ngVLA prototype antenna structure.
- Pointing characterization is by definition *indirect* in that it measures most, but not all, of the antenna's structural deformations which impact radiometric pointing performance.

it is recommended that ngVLA not consider the use of an OPT for ngVLA prototype antenna pointing characterization.

8 Path Length Stability Requirement

In the following we describe the measurement systems and techniques which we believe will allow for the proper characterization of the ngVLA 18 m antenna path length stability performance. Table 10 lists these antenna performance requirements and the requirements for the associated measurement systems that NRAO will need to develop.

Table 10: ngVLA 18 m Antenna Path Length Stability Requirements

Op Env	Req #[a]	Value	Trace[a]	Eval Prec
Path Length Stability				
Precision	ANT2501	18 μm RMS over a 5 minute period, with motion up to 5 degrees	CAL0313	3 μm

[a] See Dunbar (2020); Selina et al. (2018); Hales (2019).

8.1 Laser Interferometer Path Length Measurement

To characterize the path length stability of the ALMA prototype antennas, Greve & Mangum (2008) used an Automated Precision Incorporated (API) 5D laser interferometer. The process involved measuring the path length stability at representative places in the antenna structure, such as along the azimuth axis, ultimately building-up a total optical path stability over the specified ALMA operating conditions. Figure 14 provides a schematic showing how the API 5D laser interferometer system was used to measure the total path length through the ALMA prototype antennas. A not-so-in-depth check of laser interferometer systems today indicates that API sells a modern system[4] with linear measurement accuracy of 0.2μm/m accuracy over distances less than 45 m, sufficient to characterize the path length stability of the ngVLA prototype antenna.

9 Conclusions

In this memo we have described and derived measurement systems and techniques that can be used to verify the surface, pointing, and path length performance of the ngVLA 18 m prototype antenna.

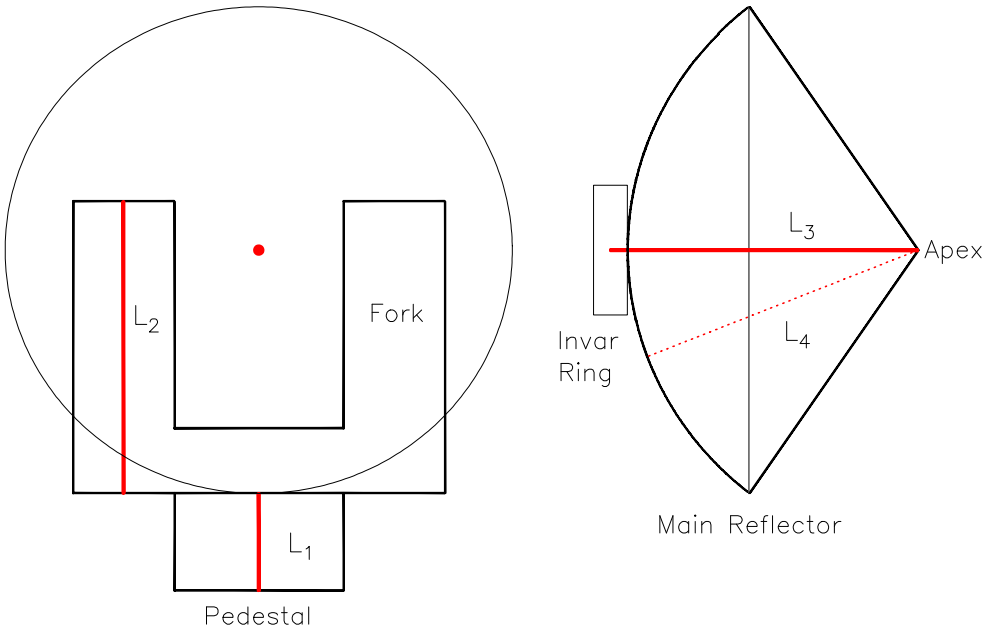

Figure 14: Schematic of the API 5D laser interferometer path length stability measurement setup for the ALMA prototype antennas.

10 Appendix A: Site Acceptance Testing List

Acknowledgements

Thanks to Bryan Butler, Rick Perley, and Todd Hunter for enlightening discussions. Bryan provided the XML file of VLA receiver temperatures that feeds the ETC. Lorant Sjouwerman provided the VLA calibrator catalog information used to assess pointing and holography target flux availability.

References

Baars, J. W. M., Lucas, R., Mangum, J. G., & Lopez-Perez, J. A. 2007, IEEE Antennas and Propagation Magazine, Volume 49, #5

Baars, J. W. M., Martin, R. N., Mangum, J. G., McMullin, J. P., & Peters, W. L. 1999, PASP, 111, 627, doi: 10.1086/316365

Butler, B. 2002, VLA Test Memo Series, Memo #232

Dunbar, D. 2020, ngVLA Technical Requirements 020.25.00.00.00-0001-REQ

EMSS. 2019, ngVLA Requirements Document 020.22.00.00.00-0001-REQ-A-ARRAY_CALIBR_STRATEGY_REQS

Greve, A., & Mangum, J. 2008, IEEE Antennas and Propagation Magazine, 50, 66, doi: 10.1109/MAP.2008.4562258

Hales, C. 2019, ngVLA Requirements Document 020.22.00.00.00-0001-REQ-A-ARRAY_CALIBR_STRATEGY_REQS

[4]See https://apimetrology.com/xd-laser/

Holst, C., Nothnagel, A., Blome, M., et al. 2015, Journal of Applied Geodesy, 9, 1, doi: 10.1515/jag-2014-0018

Hunter, T. R., Schwab, F. R., White, S. D., et al. 2011, PASP, 123, 1087, doi: 10.1086/661950

Mangum, J. G. 2017, ALMA Antenna Efficiency, Unpublished memo

Mangum, J. G., Baars, J. W. M., Greve, A., et al. 2006, PASP, 118, 1257, doi: 10.1086/508298

Mayer, C. E., Emerson, D. T., & Davis, J. H. 1994, IEEE Proceedings, 82, 756, doi: 10.1109/5.284742

Nikolic, B., Hills, R. E., & Richer, J. S. 2007a, A&A, 465, 679, doi: 10.1051/0004-6361:20065603

Nikolic, B., Prestage, R. M., Balser, D. S., Chandler, C. J., & Hills, R. E. 2007b, A&A, 465, 685, doi: 10.1051/0004-6361:20065765

Perley, R. 2021, EVLA Memo Series, Memo #212

Ruze, J. 1966, IEEE Proceedings, 54, 633

Salas, P., Marganian, P., Brandt, J., et al. 2020, in Society of Photo-Optical Instrumentation Engineers (SPIE) Conference Series, Vol. 11445, Society of Photo-Optical Instrumentation Engineers (SPIE) Conference Series, 114456C, doi: 10.1117/12.2560393

Selina, R., Murphy, E., Carilli, C., et al. 2018, ngVLA Technical Requirements 666.25.00.00.00-0001-REQ

Silver, S. 1949, Microwave Antenna Theory and Design

Sjouwerman, L. 2021, Private Communication

Table 11: ngVLA 18 m Antenna Site Acceptance Test List

Requirement #	Parameter/Requirement
	Mechanical
ANT0205	El-Boresight Axis Offset
ANT0206	Az-El Axis Offset
ANT0207	Az-Boresight Axis Offset
	Surface
ANT0501	Surface Accuracy, Precision
ANT0502	Surface Accuracy, Normal
	Pointing
ANT0611	Absolute Pointing Error, Precision
ANT0612	Referenced Pointing Error, Precision
ANT0621	Absolute Pointing Error, Normal
ANT0622	Referenced Pointing Error, Normal
	Path Length
ANT2501	Optical Path Length Drift
	Focus
ANT0702	Focus Stability, Normal
ANT0703	Focus Rotation, Normal
	Positioning
ANT0801	Azimuth Tracking Range
ANT0802	Elevation Tracking Range
ANT0901	Slew: Azimuth
ANT0902	Slew: Elevation
ANT0903	Acceleration: Azimuth
ANT0904	Acceleration: Elevation
ANT0905	Slew + Settle Time
ANT0906	Tracking: Azimuth
ANT0907	Tracking: Elevation
	Environmental
ANT1101	Resistive Losses
ANT1201	Solar Observations
ANT1411	Precision Env.: Solar Thermal Load
ANT1412	Precision Env.: Wind
ANT1413	Precision Env.: Temperature
ANT1414	Precision Env.: Temp. Rate of Change
ANT1415	Precision Env.: Precipitation
ANT1421	Normal Env.: Solar Thermal Load
ANT1422	Normal Env.: Wind
ANT1423	Normal Env.: Temperature
ANT1424	Normal Env.: Temp. Rate of Change
ANT1425	Normal Env.: Precipitation
ANT1441	Survival: Wind
ANT1442	Survival: Temperature
ANT1443	Survival: Radial Ice
ANT1444	Survival: Rain Rate
ANT1445	Survival: Snow Load - Antenna
ANT1446	Survival: Hail Stones
ANT1494	Maximum Solar Flux
ANT1495	Maximum UV Radiation

[a] See Dunbar (2020); Selina et al. (2018); Hales (2019).

[b] Note that the aperture plane error is approximately double the root sum square (RSS) of the surface error of the complete antenna optics system.